Impacts of the Lagrangian Data Assimilation of Surface Drifters on Estimating Ocean Circulation during the Gulf of Mexico Grand Lagrangian Deployment

LUYU SUN,[a] STEPHEN G. PENNY,[a,b,c] AND MATTHEW HARRISON[d]

[a] *Department of Atmospheric and Oceanic Science, University of Maryland, College Park, College Park, Maryland*
[b] *Sofar Ocean Technologies, San Francisco, California*
[c] *Cooperative Institute for Research in Environmental Sciences, University of Colorado Boulder, Boulder, Colorado*
[d] *NOAA/Geophysical Fluid Dynamical Laboratory, Princeton, New Jersey*

(Manuscript received 21 May 2021, in final form 22 January 2022)

ABSTRACT: Satellite-tracked in situ surface drifters, providing measurements of near-surface ocean quantities, have become increasingly prevalent in the global ocean observation system. However, the position data from these instruments are typically not leveraged in operational ocean data assimilation (DA) systems. In this work, the impact of an augmented-state Lagrangian data assimilation (LaDA) method using the local ensemble Kalman transform filter is investigated within a realistic regional ocean DA system. Direct positioning data of surface drifters released by the Consortium for Advanced Research on Transport of Hydrocarbon in the Environment during the summer 2012 Grand Lagrangian Deployment Experiment are assimilated using a Gulf of Mexico (GoM) configuration of the Modular Ocean Model, version 6, of the Geophysical Fluid Dynamics Laboratory. Multiple cases are tested using both 1/4° eddy-permitting and 1/12° eddy-resolving model resolutions: 1) a free running model simulation, 2) a conventional assimilation of temperature and salinity profile observations, 3) an assimilation of profiles and Lagrangian surface drifter positions, and 4) an assimilation of the profiles and derived Eulerian velocities. LaDA generally produces more accurate estimates of all fields compared to the assimilation of derived Eulerian velocities, with estimates of surface currents notably improving, when transitioning to 1/12° model resolution. In particular, LaDA produces the most accurate estimates of sea surface velocities under tropical cyclone conditions when Hurricane Isaac (2012) impacted the GoM. Further experiments applying a vertical localization while assimilating surface drifter positions improve the estimates of temperature and salinity below the mixed layer depth. Cases including the surface drifter positions in the DA show better Lagrangian predictability than the conventional DA.

KEYWORDS: Lagrangian circulation/transport; In situ oceanic observations; Kalman filters; Ensembles; Data assimilation; Nonlinear models

1. Introduction

Wind-driven surface ocean currents play a key role in storing and transferring heat energy throughout the Earth system. Due to the significant contribution of surface ocean currents to the characterization of Earth's climate (WMO 2015), ocean surface currents have been included in the list of essential climate variables (Bojinski et al. 2014). Improving the representation of surface currents has also been shown to improve estimation of hurricane intensity (Li and Toumi 2018; Zhang and Emanuel 2018; Chen and Zhang 2019; Phillipson et al. 2021). Knowledge of ocean surface velocities can benefit other applications such as optimized route planning for maritime navigation, tracking pollutants or oil spills like those produced by *Deepwater Horizon*, or assisting survival and rescue teams.

Ocean data assimilation (DA) typically produces physical state estimates by combining a numerical forecast model with sparse observations. However, producing accurate estimates of ocean velocities using DA has been a persistent challenge due to a lack of direct measurements for ocean surface currents on synoptic scales (Penny et al. 2015). Increasing model resolution exacerbates this issue, as even more observations are needed to constrain the smaller scales that are resolved. In recent years, the technologies to observe ocean currents have progressed significantly. Examples include advances in satellite-based altimetry (Scharroo et al. 2013), enhanced mooring arrays (Bailey et al. 2019), and high-frequency (HF) radar (Capodici et al. 2019). In this study, we emphasize the utilization of surface Lagrangian drifters. Surface drifters provide the most feasible means of obtaining spatially distributed simultaneous measurements of the structure of the ocean's surface velocity field on length scales from 100 m to 10 km (Poje et al. 2014; Haza et al. 2014; Mohamad and Majda 2020; Pearson et al. 2019).

A variety of methods have been applied to improve ocean current estimation by assimilating surface drifter measurements under realistic scenarios for regional ocean scales (Isern-Fontanet et al. 2017). Three primary strategies have been used to assimilate surface drifters using the Lagrangian nature of the drifter device (i.e., consisting of position-time measurements). The first, denoted as the Eulerian approach (or "pseudo-Lagrangian"), converts a series of Lagrangian positions into Eulerian velocity by determining the change in drifter position over some time scale (Hernandez et al. 1995; Ishikawa et al. 1996; Toner et al. 2001a,b). This approach, in combination with assimilating temperature and salinity observations from other instruments, is straightforward to implement in existing operational ocean DA frameworks, and has

Corresponding author: Luyu Sun, lysun@umd.edu

DOI: 10.1175/MWR-D-21-0123.1

been applied in many regions, such as the Gulf of Mexico (Jacobs et al. 2014; Carrier et al. 2014, 2016; Muscarella et al. 2015; Coelho et al. 2015), the Indian Ocean (Santoki et al. 2012, 2013) and the Angola Basin (Phillipson and Toumi 2017). All these studies have shown significant improvements in estimating ocean currents after including the assimilation of the "proxy" surface velocity data measured from drifter devices. The second approach directly assimilates the Lagrangian data by minimizing the distance between the observed trajectories and the synthetic trajectories generated by the model velocity field (Molcard et al. 2003, 2005; Özgökmen et al. 2003; Taillandier et al. 2006; Nodet 2006; Nilsson et al. 2012). For instance, the Lagrangian variational analysis (LAVA) method proposed by Taillandier et al. (2006) has been successfully used by Berta et al. (2015) to restore ageostrophic contributions beyond the simple Ekman model. The third approach is fully Lagrangian, in which the system state vector is extended by including the original fluid states and the augmented drifter state variables (Ide et al. 2002; Kuznetsov et al. 2003; Sun and Penny 2019). The third approach has not yet been applied in a realistic setting, and this will be our focus here.

Different DA methods have been proposed within the framework of augmented-state Lagrangian DA (LaDA) and all of them have shown promising results using the identical twin approach of observing system simulation experiments (OSSEs). Previous attempts within this LaDA category were designed based on the Kalman filter. For example, Ide et al. (2002) and Kuznetsov et al. (2003) examined the extended Kalman filter (Jazwinski 1970) for applications of the augmented-state LaDA within point-vortex systems. Salman et al. (2006), Apte et al. (2008), and Vernieres et al. (2011) extended the examination of this LaDA approach using the ensemble Kalman filter (EnKF; Evensen 2004) to more realistic ocean systems, such as a linear shallow water system and a multilayer reduced gravity model of the Gulf of Mexico. These methods were applied with high-dimensional model states, though the approach failed to capture dynamics with the high-order nonlinearity due to the resulting non-Gaussian distribution of error (Apte et al. 2008; Apte and Jones 2013). An alternative assimilation method that could be used in the presence of this nonlinearity is the particle filter (PF) (Spiller et al. 2008; Salman et al. 2008), but the PF does not scale well to high dimensions (Snyder et al. 2008). Slivinski et al. (2015) designed a hybrid approach combining both of the EnKF and PF to attempt to solve the problems of nonlinearity and high-dimensionality simultaneously by updating the flow states using an EnKF and the drifter states using a PF. This hybrid approach was able to alleviate the nonlinearity issue generated by the evolution of the Lagrangian paths by assimilating a single drifter in a linear shallow water model. Sun and Penny (2019) proposed a localized augment-state LaDA method based on the local ensemble transform Kalman filter (LETKF; Hunt et al. 2007). This method, denoted as LETKF-LaDA hereinafter, enabled the possibility to assimilate a large number of drifters into an advanced ocean forecast model while reducing the nonlinear impact by applying localization to both the flow states and the drifter positions. The "identical twin" approach of OSSEs were applied assessing the impact of LETKF-LaDA and the results have shown that LaDA was able to outperform the conventional assimilation of surface in situ temperature and salinity measurements. The improvements were seen not only in the surface state estimate, but also throughout the ocean column to the deeper ocean.

This study extends the work of Sun and Penny (2019) and examines the LETKF-LaDA in a realistic scenario, which is a first validation of augmented-state LaDA using historical data and a realistic numerical ocean model. This is also the first attempt in a realistic application to combine the augmented-state LaDA of drifter measurements with conventional assimilation of in situ profile measurements of temperature and salinity. We focus on the Gulf of Mexico (GoM), in which the ocean circulation, such as the Loop Current system, plays a crucial role in many critical weather events such as severe tropical storms and tropical cyclones. Carrier et al. (2014) performed a similar study using drifter measurements and they have shown that adding the drifter observations in the ocean DA greatly improves the characterization of the circulation. Instead of assimilating the direct drifter positions from the GLAD dataset, they assimilated the approximated Eulerian velocity together with profile temperature and salinity measurement, but further included remotely sensed observations (e.g., satellite SST), which occupied a vast majority of the total observations. Other differences include the observation window and DA method, which is 6 h using LETKF-LaDA for both the observation and DA windows in our work, compared to 1 h using 4D-Var with a 48-h DA window in the work of Carrier et al. (2014).

The remainder is organized as follows: section 2 reviews the augmented-state LaDA approach and introduces the corresponding analysis system; the regional forecast model and observation database are discussed in section 3; the design of experiments is described in section 4; section 5 presents the results of the aforementioned experiments; and section 6 summarizes our conclusions and directions for future research.

2. Analysis system including Lagrangian data assimilation (LaDA)

a. *Augmented-state LaDA*

The augmented-state approach (Ide et al. 2002) extends the state of the system with additional information carried by Lagrangian tracers:

$$\mathbf{x} = \begin{bmatrix} \mathbf{x}_F \\ \mathbf{x}_D \end{bmatrix}, \tag{1}$$

where $\mathbf{x}_D$ contains direct measurements from drifter devices, such as longitude, latitude, depth, temperature, and salinity, if the corresponding measurement sensors are attached. The forecast fluid model state vector $\mathbf{x}_F$ has N components containing gridded ocean states, such as temperature, salinity, and current velocity fields. In this study, we only consider the scenario of drifter data consisting of positioning measurements of longitude and latitude, and assume that the drifters maintain a constant depth. In this case, if there are N_D forecasting drifters then $\mathbf{x}_D$ is a state vector of $2N_D$ components,

with each drifter containing two measurements: longitude and latitude. The drifter advection equation is then added to the original fluid dynamical system as

$$\begin{cases} \dfrac{d\mathbf{x}_F^f}{dt} = M_F\left(\mathbf{x}_F^f,\ t\right) \\ \dfrac{d\mathbf{x}_D^f}{dt} = M_D\left(\mathbf{x}_F^f,\ \mathbf{x}_D^f,\ t\right) \end{cases}, \tag{2}$$

where M_F is the numerical ocean model. The term M_D is the extended drifter simulation dynamics operator, such as the offline operator OceanParcels, v2.0.0 (Delandmeter and van Sebille 2019) or the online drifter modules in advanced ocean models such as the Hybrid Coordinate Ocean Model (HYCOM; Wallcraft et al. 2009) and Modular Ocean Model, version 6 (MOM6; NOAA-GFDL 2021).

To assimilate the drifter measurements simultaneously with conventional temperature and salinity (T, S) profile observations, we formulate the observation operator as

$$\begin{bmatrix} \mathbf{y}_{T,S}^o \\ \mathbf{y}_D^o \end{bmatrix} = \begin{bmatrix} \mathbf{H}_F & 0 \\ 0 & \mathbf{H}_D \end{bmatrix} \begin{bmatrix} \mathbf{x}_F^t \\ \mathbf{x}_D^t \end{bmatrix} + \varepsilon = \mathbf{H}\mathbf{x}^t + \varepsilon, \tag{3}$$

where

$$\mathbf{H} = \begin{bmatrix} \mathbf{H}_F & 0 \\ 0 & \mathbf{H}_D \end{bmatrix} \text{ and } \varepsilon \sim N(0,\ \mathbf{R}) \cdot \tag{4}$$

Suppose there are L profile measurements and L_D drifter positions observed, then the temperature and salinity profile observations $\mathbf{y}_{T,S}^o$ is an L-dimensional vector and the longitude and latitude measurements of drifters $\mathbf{y}_D^o$ a $2L_D$-dimensional vector. A linear observation operator assimilating drifter positions $\mathbf{H}_D$ is $2L_D \times 2N_D$ with diagonal entries either 1 or 0. If the ID number of the simulated drifter coincides with the observed drifter ID number, then the associated entries are designated as 1, otherwise are 0. Matrix $\mathbf{H}_F$ is $L \times N$, a standard linear observation operator assimilating in situ temperature and salinity observations mapping from gridded model space to observation space. Parameter ε is a Gaussian observation error, with observation error covariance $\mathbf{R}$. The augmented-state LaDA approach provides an estimator $\mathbf{x} = (\mathbf{x}_F \mathbf{x}_D)^{\mathrm{T}}$ given the observations $\mathbf{y}^o$. With the Gaussian assumption, the Kalman filter based methods attempt to provide the best linear unbiased estimator by taking advantage of the estimated observation error covariance matrix $\mathbf{R}$ and the estimated background error covariance matrix of the combined fluid and drifter states defined as

$$\mathbf{P} = \begin{bmatrix} \mathbf{P}_{\mathrm{FF}} & \mathbf{P}_{\mathrm{FD}} \\ \mathbf{P}_{\mathrm{FD}}^{\mathrm{T}} & \mathbf{P}_{\mathrm{DD}} \end{bmatrix}, \tag{5}$$

where $\mathbf{P}_{\mathrm{FF}}$ and $\mathbf{P}_{\mathrm{DD}}$ define the background error covariance matrices of the fluid state vector and the drifters state vector, respectively. The matrix $\mathbf{P}_{\mathrm{FD}}$ is denoted as the cross-covariance matrix of the background errors for the fluid and drifters state vectors. In particular, the prior error covariance matrix of an EnKF is determined by the sample error covariance matrix from ensemble forecast perturbations around the ensemble mean at each DA cycle.

b. Local ensemble transform Kalman filter (LETKF)

Extending the approach based on the works by Bishop et al. (2001) and Hamill et al. (2001), the local ensemble transform Kalman filter (LETKF) proposed by Hunt et al. (2007) is a type of ensemble square root filter that uses the localization approach of Ott et al. (2004). The linear transform within the LETKF updates the analysis ensemble deterministically by shifting different ensemble members from the prior distribution to the posterior distribution. The LETKF is scaled for realistic systems by applying a combination of localization and parallelization, through performing the calculation of the analysis independently at each grid point. Localization is one of the primary tools for scaling DA methods for use with spatially extended high-dimensional nonlinear systems. There are generally two types of localization used by DA methods: observation space (R-localization), and model space (B-localization) (Greybush et al. 2011). LETKF employs R-localization by selecting and weighting local observations in a prescribed region around each grid point while excluding observations outside this region. This type of localization permits the analysis to be formed from an effectively larger dimensional space than could be determined by forming the transform operator directly from a linear combination of global perturbations, though each localized solution is still determined from a linear subspace that is limited by the ensemble size.

The LETKF-LaDA (Sun and Penny 2019) is an augmented-state LaDA using LETKF, which allows for the assimilation of multiple drifter measurements. To assimilate the conventional in situ profile observations together with the Lagrangian observations, the definition of the localization region remains the same as the original LETKF algorithm. However, the observation operator defined for each localization region must be modified according to the formula in Eq. (3), which contains the localized linear observation operator for both the temperature and salinity profiles (i.e., $\mathbf{H}_{F[l]}$) and the drifter measurements (i.e., $\mathbf{H}_{D[l]}$), where the subscript "$[l]$" indicates a localized component. This modification allows for defining parameters such as the localized observation error covariance matrix $\mathbf{R}_{[l]}$ and the localized forecast perturbation matrix $\mathbf{Y}_{[l]}^f = \mathbf{H}_{[l]}\mathbf{X}_{[l]}^f$ within the observation space. The localized observation vector $\mathbf{y}_{[l]}^o$ and the localized forecast ensemble mean $\overline{\mathbf{y}}_{[l]}^f$ are also formed, and can contain a mixture of both conventional profile and drifter components. The localized analysis error covariance and weight matrices can then be determined as

$$\tilde{\mathbf{P}}_{[l]}^a = \left[\frac{(K-1)}{\rho}\mathbf{I} + \left(\mathbf{Y}_{[l]}^f\right)^{\mathrm{T}}\mathbf{R}_{[l]}^{-1}\mathbf{Y}_{[l]}^f\right]^{-1},\ \mathbf{W}_{[l]}^a = \left[(K-1)\tilde{\mathbf{P}}_{[l]}^a\right]^{1/2}, \tag{6}$$

where K is the ensemble size, ρ is the multiplicative covariance inflation factor, and is held fixed at $\rho = 1.0$ throughout this work. The mean ensemble weight vector is derived as

$$\overline{\mathbf{w}}_{[l]}^a = \tilde{\mathbf{P}}_{[l]}^a\left(\mathbf{Y}_{[l]}^f\right)^{\mathrm{T}}\mathbf{R}_{[l]}^{-1}\left(\mathbf{y}_{[l]}^o - \overline{\mathbf{y}}_{[l]}^f\right). \tag{7}$$

The analysis ensemble members are calculated using

$$\mathbf{x}_{[l]}^{a(k)} = \overline{\mathbf{x}}_{[l]}^{f} + \mathbf{X}_{[l]}^{f}\mathbf{w}_{[l]}^{a(k)}, \tag{8}$$

where superscript k is the index for the ensemble member and $\left\{\mathbf{w}_{[l]}^{a(k)}\right\}$ is determined by columns of a resulting matrix by adding $\overline{\mathbf{w}}_{[l]}^{a}$ to each column of $\mathbf{W}_{[l]}^{a}$.

3. Forecast model and observations

a. Model description

MOM6 is the latest generation ocean model developed by the Geophysical Fluid Dynamics Laboratory (GFDL). Major improvements over previous versions include the general-coordinate formation, conservative representation of wetting and drying, and the novel parameterization of subgrid scale physics (Griffes et al. 2015). The ocean model source code is taken from the open source project MOM6 (git@github.com:NOAA-GFDL/MOM6.git), which is a collaborative software development project for a generalized finite volume representation of the ocean suitable for short-term to climate scale study (Adcroft et al. 2019). An online parallel memory Lagrangian tracking algorithm was used to simulate observed drifter trajectories. Lateral open boundary conditions at the open edges of the model domain are handled by incorporating barotropic (Flather and Heaps 1975) and baroclinic (Orlanski 1976) radiation schemes.

The model domain is defined in a region extending 18°–30.5°N and 262°–279.5°E using spherical coordinates. Two primary horizontal resolutions are tested: an eddy-permitting configuration of 1/4° (roughly 24 km) and an eddy-resolving configuration of 1/12° (roughly 8 km). The horizontal grid and the bathymetry are generated by interpolating from the gridded bathymetric dataset of General Bathymetric Chart of the Oceans (GEBCO). We apply the same 1/4° bathymetry file for both horizontal grid resolutions in order to more cleanly assess the impact of increasing ocean resolution by not simultaneously changing the bathymetric representation. A total of 75 levels defined with z^* coordinates are used in the vertical with 2–3-m resolution in the top 50 m. The ocean model integration step is chosen as 150 s. Ensemble surface atmospheric forcing is provided by the twentieth century Reanalysis version 3 (20CRv3) for surface winds, temperature, specific heat, precipitation, pressure and downward shortwave and longwave radiation with an updating frequency of 3 h (Slivinski et al. 2019). The forcing for each ocean ensemble member is selected from a corresponding member forcing within the 80-member 20CRv3 ensemble dataset. The open boundary conditions (OBC) for the eastern and southern boundaries are determined by the Simple Ocean Data Assimilation version 3.4.2 (SODAv3.4.2; Carton et al. 2018a,b) updated monthly, and are identical for all ensemble members.

b. Grand Lagrangian Deployment and World Ocean Database 2018

During the summer of 2012, the Consortium for Advance Research on Transport of Hydrocarbon in the Environment (CARTHE) conducted experiments of the Grand Lagrangian Deployment (GLAD) by deploying 297 CODE-type surface drifters (centered at a depth of one meter) tracked in real time using SPOT GPS units. Drifters in the GLAD program, without any temperature or salinity sensors attached, were gradually launched starting on 20 July 2012 and drifted with the surface ocean currents through 22 October 2012. Both the launching and terminating processes were completed over a span of multiple days.

In this work, we use the publicly available dataset produced by the GLAD experiments generated by Özgökmen (2013). The data were processed using a fourth-order Butterworth low-pass filter with subsampling at uniform 15-min intervals. The instantaneous drifter position entries are assimilated using the augmented-state LaDA, while the corresponding derived velocity entries are assimilated using the Eulerian approach as a comparison. These derived velocities were approximated using the average rates of changing displacement within the 15-min intervals. Figure 1a shows the GPS drifter positions on 1 August 2012, when the launching process for all the drifters was already completed.

In situ temperature and salinity profile observations that are available in the GoM during the examination period are provided by the World Ocean Database 2018 (WOD18) (Fig. 1c). This dataset contains measurements collected from profiling float (PFL), expendable bathythermographs (XBT), conductivity–temperature–depth probes (CTD), ocean station data (OSD), gliders (GLD) etc. Data entries are flagged in the original WOD18 if they fail quality control checks (Garcia et al. 2018). In this study, all observations marked with a negative quality control flag (e.g., failing annual/seasonal/monthly standard deviation check) are withheld from the analysis in order to avoid negative impacts caused by outlier measurements. Sun and Penny (2019) indicated strong correlations in the error statistics of sea surface height (SSH) and simulated drifter positions in an idealized model. To highlight the impact of drifter measurements on ocean currents, no measurements related to SSH are assimilated in any of the DA approaches within this work. The joint assimilation of SSH and surface drifter measurements remains an open research problem.

4. Experiment design

We select 0000 UTC 1 August–2359 UTC 29 September 2012 as the examination time period for this study, corresponding with the period the GLAD field campaign was conducted in the GoM. All subsequent times are reported as coordinated universal time (UTC). Within this time period, the loop current eddy has already been shed from the loop current and is located near the central GoM (roughly at 27°N, 271°E. Carrier et al. 2014; Coelho et al. 2015). Hurricane Isaac crossed the GoM during 26–30 August with the category 1 intensity, producing winds above 25 m s^{-1} and very high surface drifter velocities above 2 m s^{-1} (Coelho et al. 2015). As shown in Fig. 1d, the average kinetic energy of the observing drifters peaks during this time, inferring fast advective underlying surface currents driven by the strong wind of the hurricane. The tropical cyclone additionally led to a sharp drop in

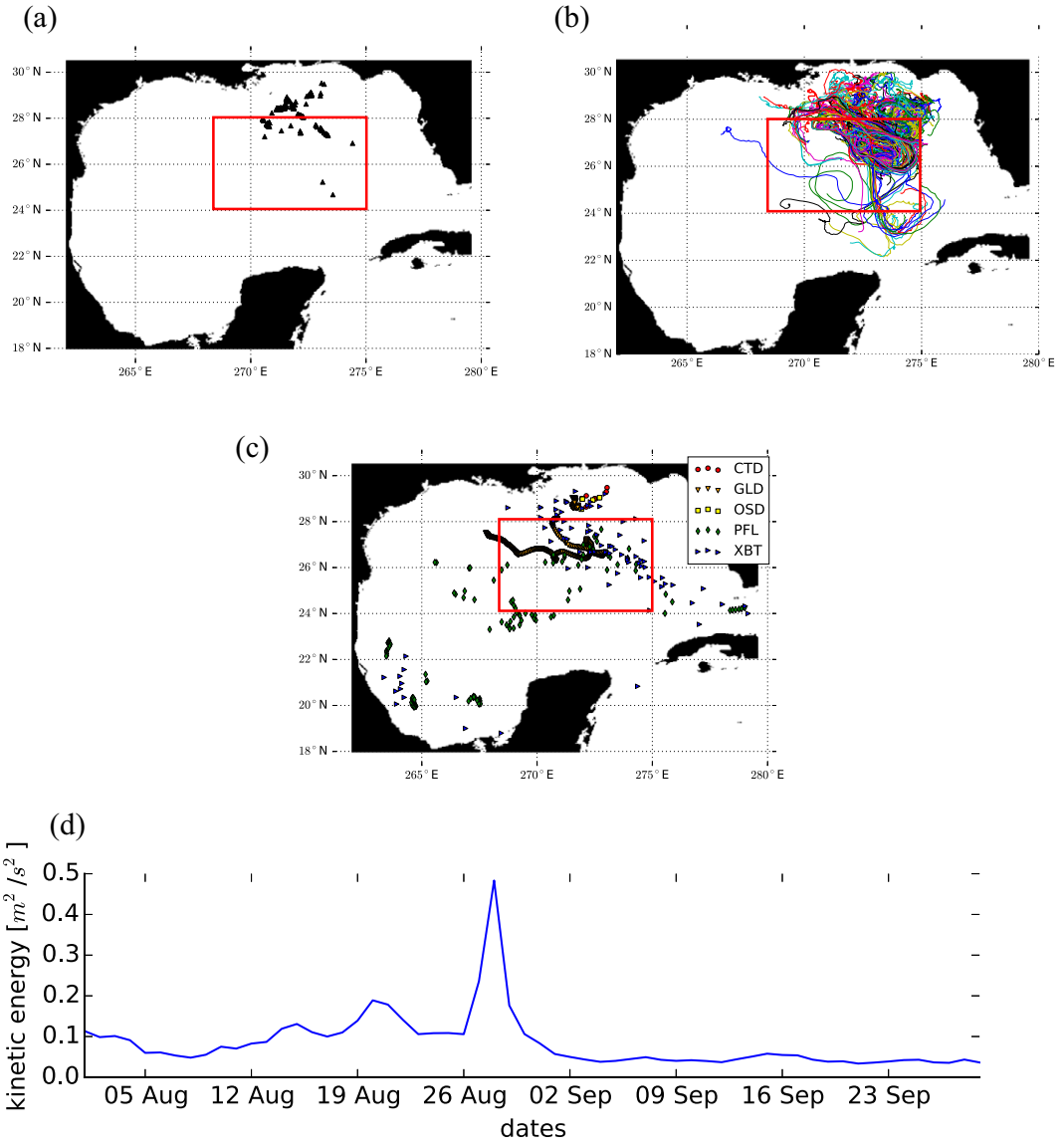

FIG. 1. (a) 297 drifter GPS locations recorded in GLAD database on 1 Aug 2012. (b) 132 drifter trajectories that are present for the entire examination period. (c) Locations of PRL, XBT, CTD, OSD, and GLD from 1 Aug to 29 Sep 2012 (observations plotted at a daily interval). The red box highlights the region for the computation of RMSEs. (d) Time variation of average kinetic energy among all the observing drifters.

the number of reporting drifters (Muscarella et al. 2015) and there are 132 drifters remaining at the end of the examination period (see Fig. 1b).

To produce a reasonable set of initial conditions for the ocean ensemble at 0000 UTC 1 August 2012 for different forecast systems (i.e., 1/4° and 1/12°) correspondingly, an ensemble spinup procedure was conducted from the beginning of January to the end of July (0000 UTC 1 January–2359 UTC 31 July). Ensemble members (1–30) at 1/4° resolution were initialized uniformly with the potential temperature and salinity from SODAv3.4.2 at 0000 UTC 1 Jan 2012 and embedded with the same prescribed OBC as indicated in the previous section. Each member (No. 1–30) is forced with the corresponding ensemble member of the atmospheric forcing from the 20CRv3 (No. 1–30), and is integrated for 7 months from 0000 UTC 1 January to 2359 UTC 31 July, when the ensemble spread appears fully saturated. For the spinup process of the ensemble at 1/12° horizontal resolution, the corresponding ensemble models are initialized with the interpolated 1/4° ensemble at 0000 UTC 1 July 2012 instead of the potential temperature and salinity from SODAv3.4.2 at 0000 UTC 1 January 2012. Similar to the spinup process of 1/4°, the ensemble members at 1/12° resolution are integrated using the ensemble atmospheric forcing from the 20CRv3 and the same OBC until 2359 UTC 31 July before the initiation of the DA experiments.

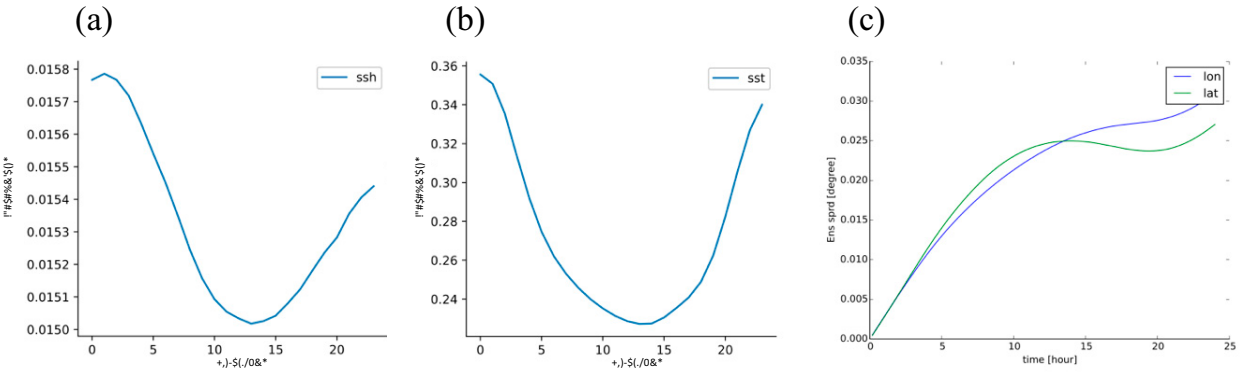

FIG. 2. The change of the spatially averaged ensemble spread for model states (a) SSH and (b) SST within the first 24-h forecast model run in the 1/12° model resolution configuration. (c) The change of the averaged ensemble spread for all simulated drifter states within the first 24 h.

The LETKF/LETKF-LaDA algorithms are used for all the DA runs, using an ensemble size of 30 members (i.e., $K = 30$). All DA experiments use 6-h assimilation windows through the study period. The choice of a 6-h DA window is determined by examining a quasi-linear growth trend of the simulated ensemble spread in SSH, sea surface temperature (SST), and drifter position (longitude/latitude) within the first 24-h forecast model run (see Fig. 2), to avoid the underfitting issue. The horizontal localization radius is set initially at double the size of the Rossby radius of deformation (Chelton et al. 1998) for both the profile and the surface drifter measurements. Each observation is assigned a spatiotemporally static estimated error. The estimated errors are set at 2.0°C for temperature, 1.0 psu for salinity, 0.08° longitude/latitude for surface drifter positions, and 0.08 m s^{-1} in "proxy" drifter zonal/meridional velocity. To reduce the effects of nonlinear error growth and prevent additional analysis drifter bias from influencing the DA performance (Salman 2008a,b), the initial drifter positions at the beginning of each 6-h time window are relocated by using the observed drifter positions, and the forecast ensemble drifter positions are generated by integrating the analysis flow ensemble at the end of previous DA step.

For both the eddy-permitting 1/4° and eddy-resolving 1/12° model configurations, three DA experiments are conducted and compared with a free model integration (denoted as FREE): 1) assimilating only the in situ temperature and salinity profile measurements from WOD18 (denoted as PROF) 2) simultaneously assimilating both the in situ temperature and salinity profile observations as well as the surface drifter GPS locations (denoted as BOTH), and 3) simultaneously assimilating both of the temperature and salinity profiles as well as the derived drifter "proxy" Eulerian velocities (denoted as BOTHvel). The free run is integrated using an identical forecast model, but is forced with the prescribed mean atmosphere forcing in 20CRv3 (among the total 80 members). A vertical localization (denoted as VLOC) depending on the mixed layer depth (MLD) is included and discussed in section 5c.

To highlight the impact of adding the assimilation of surface drifter positions, the simultaneous assimilation of in situ profiles and drifter positions (BOTH) is first compared with the free model integration (FREE) and the assimilation of only profile measurements (PROF) in section 5a. As a comparison between two main strategies of assimilating drifter measurements, the assessments of DA experiments BOTH (augmented-state approach) and BOTHvel (Eulerian approach) are investigated in section 5b. Section 5c evaluates the influence of adding the vertical localization to the assimilation of surface drifter positions (VLOC) by comparing its results with those of BOTH and PROF.

To evaluate the performance of the DA system, prior to assimilating observations, the forecast fit to the observations (also known as the innovation or departure) is examined at each DA cycle by computing the root-mean-square error (RMSE) between the forecast states and observations:

$$\mathrm{RMSE} = \sqrt{\frac{1}{K}\sum_{k=1}^{K}\left(\mathbf{y}^{o} - \mathbf{H}\mathbf{x}_{k}^{f}\right)^{2}}, \tag{9}$$

where K is the ensemble size, $\mathbf{x}_k^f$ the kth forecast ensemble member and $\mathbf{H}$ the global observation operator at the current time step as defined in Eq. (4). All RMSEs are computed within the region from 24° to 28°N and from 267° to 275°E (Figs. 1a–c), where both the WOD18 and GLAD datasets have more dense observations during the experiment period.

The skill score is then applied for evaluating the relative RMSE of one experiment based on the RMSE of another reference experiment:

$$\mathrm{SS} = 1.0 - \frac{\mathrm{RMSE}_2}{\mathrm{RMSE}_1}, \tag{10}$$

where RMSE_1 is computed for the reference experiment (e.g., FREE) and RMSE_2 is computed for the experiment of interest (e.g., PROF, BOTH, etc.). If the experiment of interest has lower RMSE than the reference experiment, the skill score metric will be positive. On the other hand, the skill metric will be negative as the experiment generates higher RMSE than the reference experiment. If there is no significant change, then the skill score value will be close to zero. We first compare the performance of each DA experiment

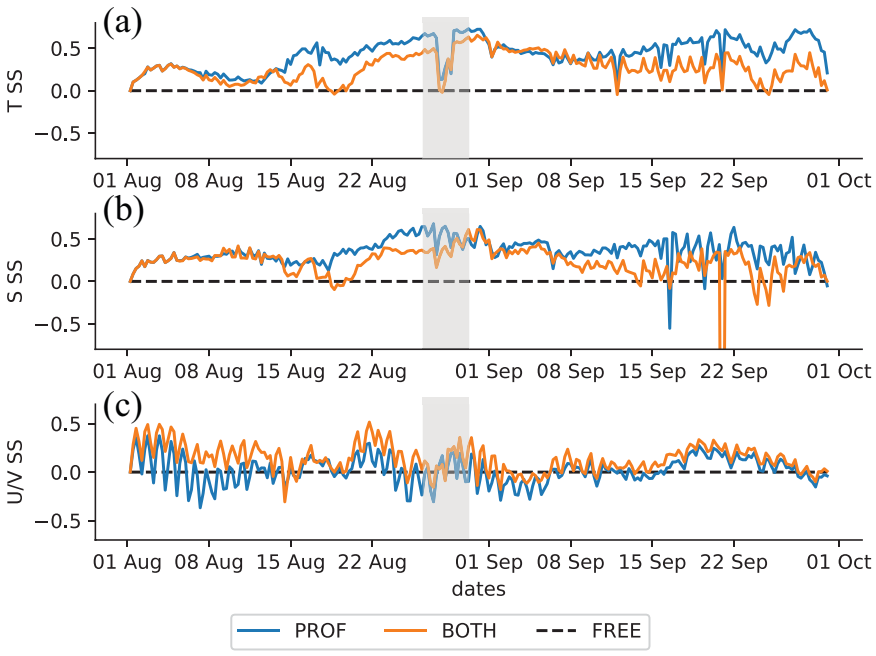

FIG. 3. Time variation of the forecast skill score measured against free run solution (black dashed line) in the 1/4° system for (a) temperature, (b) salinity, and (c) kinetic energy. Two DA runs are shown: assimilation of temperature and salinity profiles (blue line, labeled as "PROF"), and assimilation of temperature and salinity profiles and drifter positions (orange line, labeled as "BOTH"). The RMSEs defining these skill scores are computed using the errors between forecast states and observations at all heights/vertical levels. Valid from 1 Aug to 29 Sep 2012. The gray shadows in all panels represent the time region for Hurricane Isaac (26–30 Aug 2012).

(e.g., PROF, BOTH) by using the skill score relative to FREE run. The skill score of experiment BOTH relative to experiment BOTHvel is then examined to emphasize the impacts of using the augmented-state LaDA versus the Eulerian approach.

5. Results

a. *Forecasts in eddy-permitting and eddy-resolving systems*

Using the 1/4° horizontal resolution eddy-permitting model configuration, the assimilation experiments PROF and BOTH produce improvements in temperature and salinity compared with the FREE run (Figs. 3a,b and Table 1). Assimilating only temperature and salinity profiles (PROF) results in higher accuracy in estimates of subsurface temperature and salinity after 13 days, compared to assimilating both profiles and drifter positions (BOTH). [As shown in Figs. 13a,b and Table 3, BOTH typically generates smaller forecast ensemble spreads in temperature and salinity (i.e., 0.13°C and 0.026 psu) than PROF (i.e., 0.17°C and 0.036 psu) through adding more observations to constrain the fluid states. As shown in Table 3, the forecast ensemble spread of PROF in temperature is approximately one-seventh of the forecast RMSE, while the one in salinity is about one-fifth of the RMSE. Likewise, the forecast ensemble spreads of BOTH in temperature and salinity are approximately one-tenth of the corresponding forecast RMSEs (see Table 3).] Assimilating the additional drifter position measurements (BOTH) provides a more accurate forecast of the ocean velocity states (Fig. 3c), compared to assimilating only temperature and salinity profiles (PROF). The time average velocity skill score of BOTH is 0.13, which is much larger than the 0.02 skill score for the experiment of assimilating only the temperature and salinity profiles (PROF). This infers that BOTH makes prominent improvements in forecasting the velocity than PROF.

The reduced forecast accuracy of temperature and salinity in BOTH compared to the PROF experiment is apparent in the vertical RMSE comparisons along different depth levels (Fig. 4). Roughly below the MLD (approximately 150 m), the assimilation of additional surface drifter observations results

TABLE 1. The 95% confidence interval of RMSEs for experiments in the 1/4° system. The statistics are computed from the 240 sample forecast errors from 1 Aug to 29 Sep 2012. Each entry is shown in the form of $A \pm B$, where A is the sample mean and B is the standard error ($B = 1.96 \times s/\sqrt{239}$, with s being the sample standard deviation).

	FREE	PROF	BOTH	VLOC
1/4° T (°C)	2.11 ± 0.14	1.17 ± 0.09	1.47 ± 0.08	1.21 ± 0.08
1/4° S (psu)	0.31 ± 0.02	0.19 ± 0.01	0.23 ± 0.02	0.21 ± 0.02
1/4° U/V (m s^{-1})	0.29 ± 0.02	0.28 ± 0.02	0.25 ± 0.02	0.26 ± 0.02

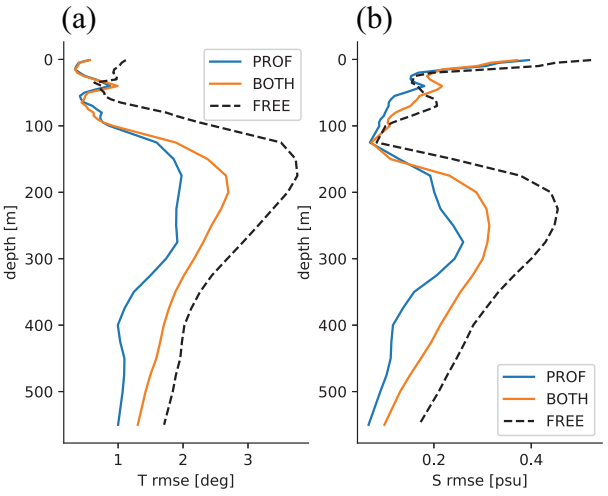

FIG. 4. Vertical RMSEs averaged through the entire experiment period (i.e., 60 days or DA cycles from 1 Aug to 29 Sep 2012) in the 1/4° system for (a) temperature and (b) salinity for three experiment cases: free run (black dashed line), assimilation of temperature and salinity profiles (blue line), and assimilation of temperature and salinity profiles and drifter positions (orange line).

in larger RMSEs than when assimilating only the temperature and salinity profiles. Above the 150-m depth, PROF experiment also slightly outperforms BOTH in salinity at most of the depth levels. These results imply that while assimilating Lagrangian drifter positions can enhance the estimation of the synoptic surface velocity when using an eddy-permitting model, additional steps must be taken to avoid degrading the analysis derived from in situ profiles. Such additional steps will be described in section 5c.

The number of observations needed to constrain a system is related to the number of nonnegative Lyapunov exponents in the system (e.g., Trevisan et al. 2010; Trevisan and Palatella 2011; Palatella 2013; Penny et al. 2019). When increasing the horizontal resolution of the model from 1/4° to 1/12°, the number of degrees of freedom for the whole system is increased. Increasing the degrees of freedom of a model can potentially increase the resolved instabilities and can affect the number of nonnegative Lyapunov exponents of the system (e.g., De Cruz et al. 2018). Therefore, more observations may be required to constrain the unstable error propagation for a model system with high resolution. As shown in Fig. 5c, the velocity skill score is constantly larger during the entire examination period when assimilating both drifter positions and profiles (BOTH) than when assimilating only profiles (PROF). The average velocity skill score of PROF is −0.07 due to its poor performance after 31 days, while adding the assimilation of surface drifter positions provides an average 0.17 velocity skill score. This improvement of BOTH in estimating the velocity over PROF in the eddy-resolving configuration is more significant than in the eddy-permitting system (see Table 1 and Table 2). This is probably because the 1/12° forecast model can resolve currents of eddy scale and provide more reasonable ensemble uncertainty in all the fluid states for the DA. The negative velocity skill scores of BOTH and

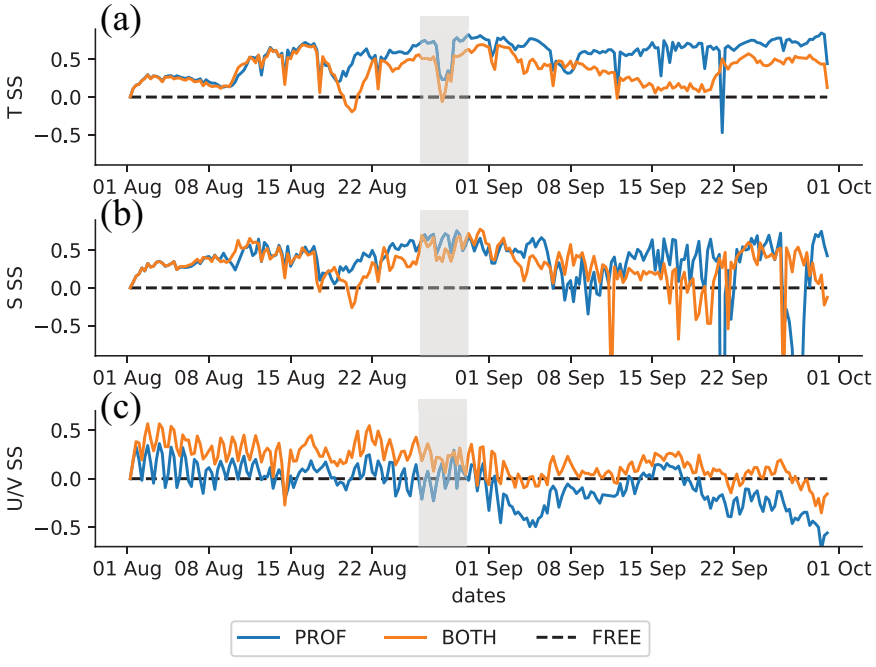

FIG. 5. As in Fig. 3, but showing the skill scores but for the 1/12° horizontal resolution model configuration. The RMSEs defining these skill scores are computed using the errors between forecast states and observations at all heights/vertical levels. The gray shadows in all panels represent the time region for Hurricane Isaac (26–30 Aug 2012).

TABLE 2. As in Table 1, but for experiments in the 1/12° system.

	FREE	PROF	BOTH	VLOC
1/12° T (°C)	2.10 ± 0.15	0.93 ± 0.11	1.29 ± 0.10	0.92 ± 0.10
1/12° S (psu)	0.31 ± 0.02	0.20 ± 0.03	0.21 ± 0.02	0.20 ± 0.02
1/12° U/V (m s^{-1})	0.31 ± 0.02	0.32 ± 0.02	0.24 ± 0.01	0.28 ± 0.02

PROF at the end of September may be caused by the dynamic change of the surface flow after Hurricane Isaac. The analysis generated by DA at 1/12° possibly introduces energy at smaller scales (than the 1/4° analysis) that somehow becomes problematic to the forecast as the hurricane passes over the area.

Similarly to the eddy-permitting model configuration, the temperature skill scores of the two DA experiments (i.e., BOTH and PROF) in the 1/12° eddy-resolving configuration are comparable in the first 18 days. After 18 Aug, however, adding the assimilation of surface drifter positions (BOTH) again degrades the forecast of subsurface temperature compared to PROF (Fig. 5a), which is statistically significant according to the 95% confidence interval in Table 2. The salinity skill scores for both of the DA experiments (i.e., BOTH and PROF) are comparable and are positive for most of the DA cycles in the first 40 days (Fig. 5b), with the assimilation of the temperature and salinity profiles (PROF) is being marginally better when comparing their averages (i.e., 0.39 for PROF and 0.36 for BOTH). After day 40 (i.e., 9 Sep), PROF and BOTH oscillate in the salinity skill score relative to FREE run. This oscillation is probably caused by a drastic decay in the number of temperature and salinity profile observations around day 38, or 7 Sep (Fig. 6), making it harder for the DA system with the high-resolution model to constrain the error perturbation compared to the DA system using the low-resolution model. Figure 7 presents the average vertical RMSEs for the two DA experiments using the 1/12° model, which shows a similar degradation of BOTH for the subsurface temperature and salinity as shown previously in the 1/4°

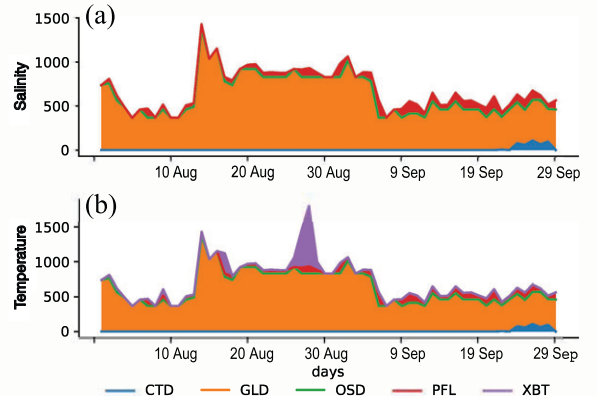

FIG. 6. The total number of different type profile observations for (a) salinity and (b) temperature from 1 Aug to 29 Sep 2012 at the Gulf of Mexico within the WOD18 database.

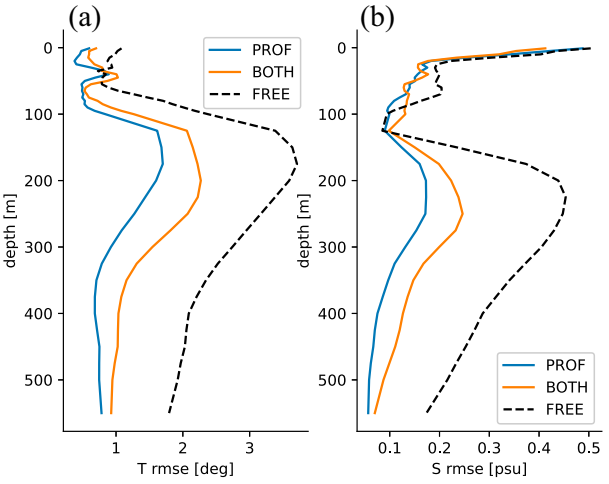

FIG. 7. As in Fig. 4, but showing the vertical RMSE but for the 1/12° horizontal resolution model configuration.

eddy permitting model. Specifically, for temperature above 150-m depth, BOTH also demonstrates degradations as compared with PROF in the 1/12° system, while the two DA approaches do not have this obvious difference in the 1/4° system as shown in Fig. 4a. Note again that this will be addressed in section 5c. The forecast ensemble spreads of BOTH in temperature and salinity (i.e., 0.20°C and 0.045 psu) are much smaller than PROF (i.e., 0.29°C and 0.068; see Table 3, Figs. 13d,e). The temperature and salinity RMSEs of BOTH are respectively 6 and 5 times larger than the corresponding temperature and salinity forecast ensemble spreads (see Table 3). Meanwhile, Table 3 also demonstrates that the prior errors of temperature and salinity in PROF are both 3 times greater than the corresponding forecast ensemble spreads.

b. *Comparison with the Eulerian approach*

We next compare the LaDA approach (BOTH) with the assimilation of derived Eulerian velocities (BOTHvel). As for the synoptic surface ocean velocity fields, assimilation of the drifter positions in the 1/4° eddy-permitting DA system provides better forecasts between 20 and 31 August 2012, though it shows negative results for 64% of all DA cycles (see Fig. 8c). Increasing the horizontal resolution improves the

TABLE 3. Time average of the forecast root-mean-square errors and total ensemble spreads of forecasts in temperature and salinity for PROF, BOTH, and VLOC at 1/4° and 1/12° DA system.

	T RMSE (°C)	T ensemble spread (°C)	S RMSE (psu)	S ensemble spread (psu)
PROF 1/4°	1.17	0.17	0.19	0.036
BOTH 1/4°	1.47	0.13	0.23	0.026
VLOC 1/4°	1.21	0.15	0.21	0.030
PROF 1/12°	0.93	0.29	0.20	0.068
BOTH 1/12°	1.29	0.20	0.21	0.045
VLOC 1/12°	0.92	0.29	0.20	0.067

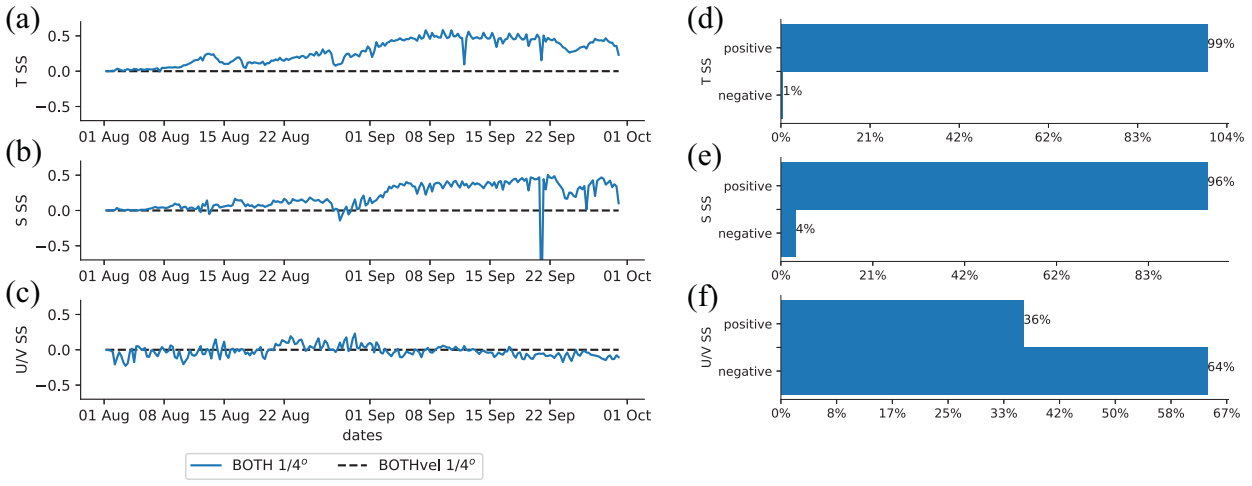

FIG. 8. Time variation of the forecast skill score (SS) for the augmented-state LaDA (blue line, "both") vs the Eulerian approach assimilating "proxy" velocities from drifters (black dashed line) for (a) temperature, (b) salinity, and (c) surface kinetic energy for 1/4° horizontal resolution model configuration. Valid from 1 Aug to 29 Sep 2012. Positive SS values indicate the LaDA is outperforming the proxy approach. (d)–(f) Histograms showing the positivity/negativity of the corresponding SS values are summarized.

relative performance of forecasting ocean surface velocities using LaDA through the entire experiment period (see Fig. 9c), especially for the period from 15 to 31 August, as LaDA reduces velocity RMSE by 18% compared to the assimilation of derived Eulerian velocities. When applied to the 1/12° eddy-resolving model, the LaDA provides a larger improvement in the estimation of ocean surface velocity fields. About 74% of all DA cycles (see Fig. 9f) outperform the assimilation of derived Eulerian velocities, as compared with 36% for the experiments using the 1/4° eddy-permitting model (see Fig. 8f). It should be noted that the ocean surface flow observed by the surface drifters moved faster during 19–31 Aug than those in other periods according to Fig. 1d. Specifically, Hurricane Isaac (2012) entered the GoM at the end of August 2012, which created a drastic change in the ocean surface circulation. This implies that the estimation error included in the observation error of the "proxy" Eulerian velocity cannot be ignored during extreme weather conditions with fast advective surface flow. The augmented-state LaDA shows a clear advantage in estimating the ocean surface velocity within the regions characterized by fast ocean currents, especially during the hurricane (i.e., 26–30 August 2012), though the observed GPS locations can still have measurement errors.

The LaDA assimilation of drifter positions outperforms the assimilation of derived Eulerian velocities when estimating 3D ocean temperature fields at different horizontal resolutions throughout the entire experiment period (Figs. 8a and 9a). The improvements are mainly concentrated below approximately 60-m depth (Figs. 10a,c). When estimating 3D ocean

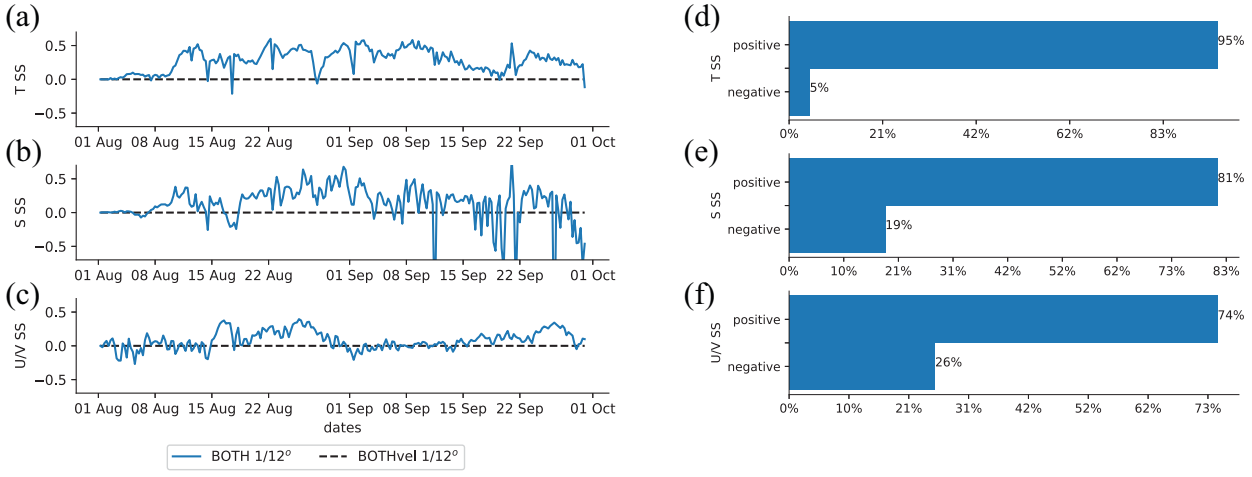

FIG. 9. As in Fig. 8, but showing the skill score and its corresponding positivity/negativity histogram for the 1/12° horizontal resolution model configuration.

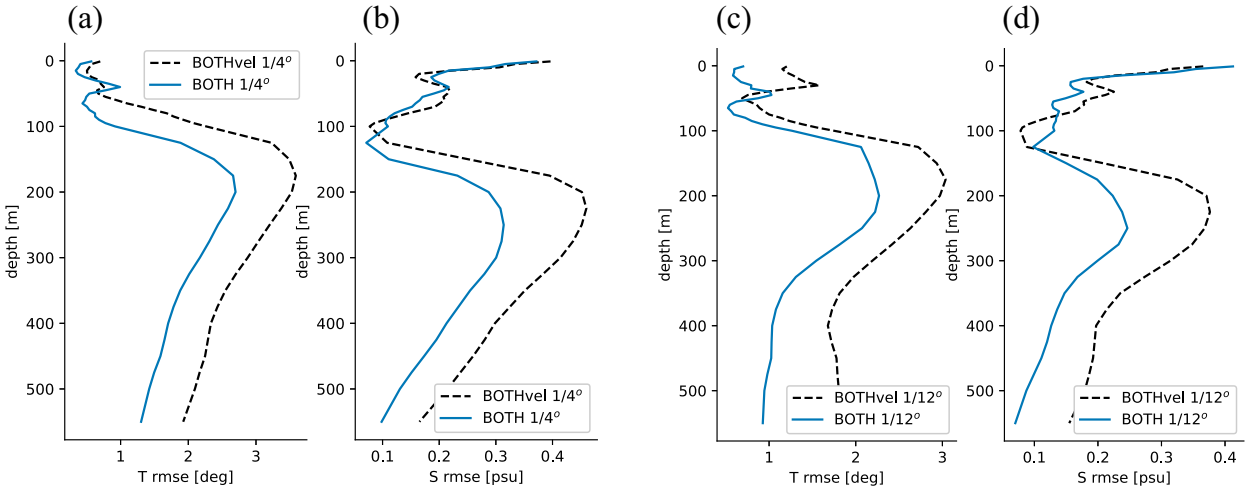

FIG. 10. Vertical RMSEs averaged through the whole time period (i.e., 60 days or DA cycles from 1 Aug to 29 Sep 2012) for temperature and salinity between experiments BOTH (blue line) and BOTHvel (black dashed line) in the 1/4° and 1/12° systems: (a) temperature RMSEs in the 1/4° system, (b) salinity RMSEs in the 1/4° system, (c) temperature RMSEs in the 1/12° system, and (d) salinity RMSEs in the 1/12° system.

salinity, the LaDA forecasts fit the salinity observations better than the Eulerian approach for almost all the DA cycles in the 1/4° (Fig. 8b), and for DA cycles before 9 September 2012 (or day 40) in the 1/12° systems (Fig. 9b). The salinity skill score of LaDA relative to the Eulerian approach oscillates in the 1/12° model after day 40 (Fig. 9b), though the LaDA outperforms in 81% of the experiment period (Fig. 9e). Further, the time average of the salinity RMSE in the LaDA experiment is lower than the Eulerian approach below 120-m depth for both the 1/4° and 1/12° configurations (Figs. 10b,d). Since both the Lagrangian and Eulerian approaches assimilate the same set of temperature and salinity observations, the differences in the errors of estimating the 3D temperature and salinity states result from the differences in error covariances related to the Lagrangian positions and the derived Eulerian velocities. This discrepancy impacts the computation of the fluid analysis ensemble spreads at each step, which then influences the formation of the fluid forecast ensemble spread at the following step. [As shown in Figs. 13a–e, there are faster degradations of forecast ensemble spreads in temperature and salinity of BOTHvel (Figs. 13a–e) than those of BOTH, which results in the underestimated model error covariances in temperature and salinity.]

c. *Adding vertical localization*

As previously mentioned in section 5a, assimilating surface drifter positions in addition to temperature and salinity profiles can degrade estimates of temperature and salinity below the MLD and even some levels above the MLD. In this section, we add a cutoff vertical localization to the assimilation of drifter positions (denoted as VLOC), which restricts the influence of surface drifter position observations to remain above the MLD, instead of the entire water column as applied in section 5a and 5b. The cutoff MLD at each time step is determined by using the ensemble mean MLD and the corresponding vertical localization function is shown as

$$f(\Delta h) = \begin{cases} 1, & \text{if } \Delta h < \overline{\text{MLD}} \\ 0, & \text{if } \Delta h \geq \overline{\text{MLD}} \end{cases},$$

where Δh is the height difference between the forecast ocean fluid states and the surface drifter observations. The $\overline{\text{MLD}}$ is the mean MLD of all the forecast ensemble members. We note that this vertical localization is only applied to the surface drifter position observations, while the conventional in situ temperature and salinity profiles still influence the ocean state estimates for the entire water column. Within the LETKF-LaDA algorithm, the mean MLD is checked at each grid point and the surface drifter observations are assimilated together with the in situ observations only for the grid points above the mean MLD.

As compared with the experiments assimilating the surface drifter positions and in situ profiles without any vertical localization (BOTH), the additional application of vertical localization (VLOC) largely enhances the estimation of temperature and salinity below the MLD for all forecast model resolutions (Figs. 11a–d and Tables 1 and 2) for both the 1/4° and 1/12° systems. With the 1/4° model resolution, adding the vertical localization (VLOC) does not generate consistently lower errors in temperature or salinity than assimilating only profile observations (PROF) below the MLD (Figs. 11a,b). Using the 1/12° model resolution, the combination of a vertically localized LaDA and conventional assimilation of profiles (VLOC) results in the lowest RMSEs for temperature and salinity at all levels below MLD among all other examined DA experiments (including PROF and BOTH) of the same forecast model resolution (Figs. 11c,d), while the errors of VLOC are comparable with PROF for temperature and salinity above MLD.

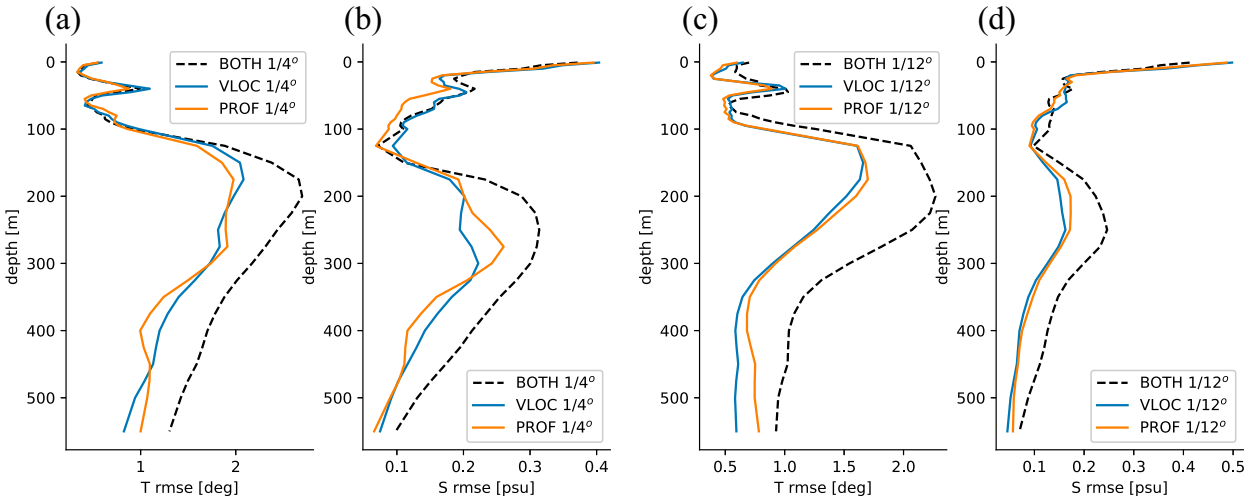

FIG. 11. Vertical RMSEs averaged through the whole time period (i.e., 60 days or DA cycles from 1 Aug to 29 Sep 2012) comparing experiments using vertical localization (VLOC; blue line) and without using vertical localization (BOTH; black dashed line). Assimilation of profiles (PROF; orange line) is shown as a reference. (a) Temperature RMSEs in the 1/4° system, (b) salinity RMSEs in the 1/4° system, (c) temperature RMSEs in the 1/12° system, and (d) salinity RMSEs in the 1/12° system.

For both the 1/4° and 1/12° horizontal resolutions in Fig. 12, adding the vertical localization (VLOC) provides less accuracy on estimating velocity fields than the one without vertical localization (BOTH). In the meantime, VLOC outperforms the assimilation of only profiles (PROF) in forecasting the velocity field under the 1/4° framework up till 8 Sep. As increasing the horizontal resolution to 1/12° system, the velocity fields generated by VLOC has better accuracy than the ones by PROF, though both are worse than the assimilation of profiles and Lagrangian drifter positions without any vertical localization (BOTH). These degradations of VLOC and PROF as compared with BOTH are statistically significant at the 95% level as shown Table 2.

In the 1/4° system, adding vertical localization (VLOC) generates forecast ensemble spread that is sandwiched between those of PROF and BOTH for all the ocean states (Figs. 13a–c, Table 3). Increasing the horizontal resolution, the forecast ensemble spread of VLOC becomes nearly as large as PROF during the whole examination time period (Figs. 13d–f, Table 3). These implies that the vertical localization on both the resolution systems can slow the degradation of ensemble spreads for all ocean states, which

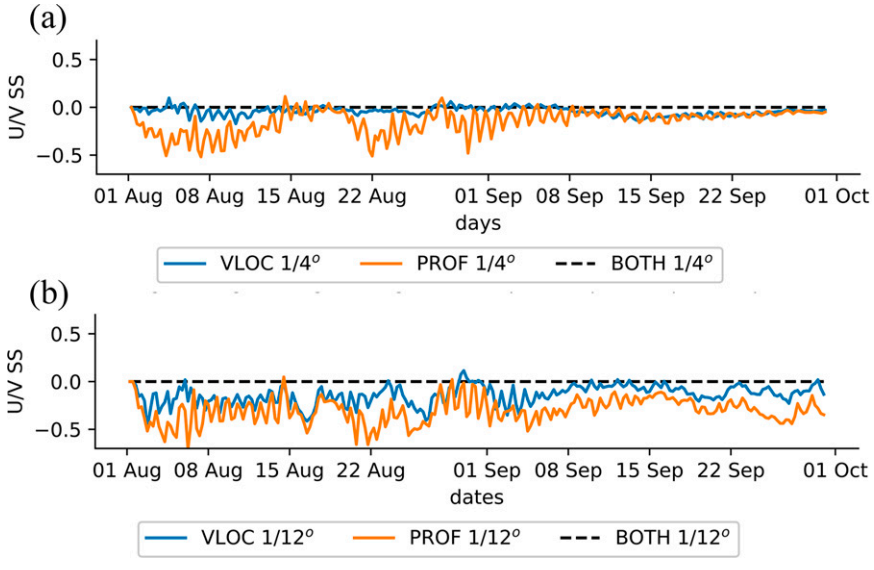

FIG. 12. Time variation of the forecast velocity skill score (SS) of VLOC and PROF measured against BOTH (black dashed line) in the (a) 1/4° and (b) 1/12° system.

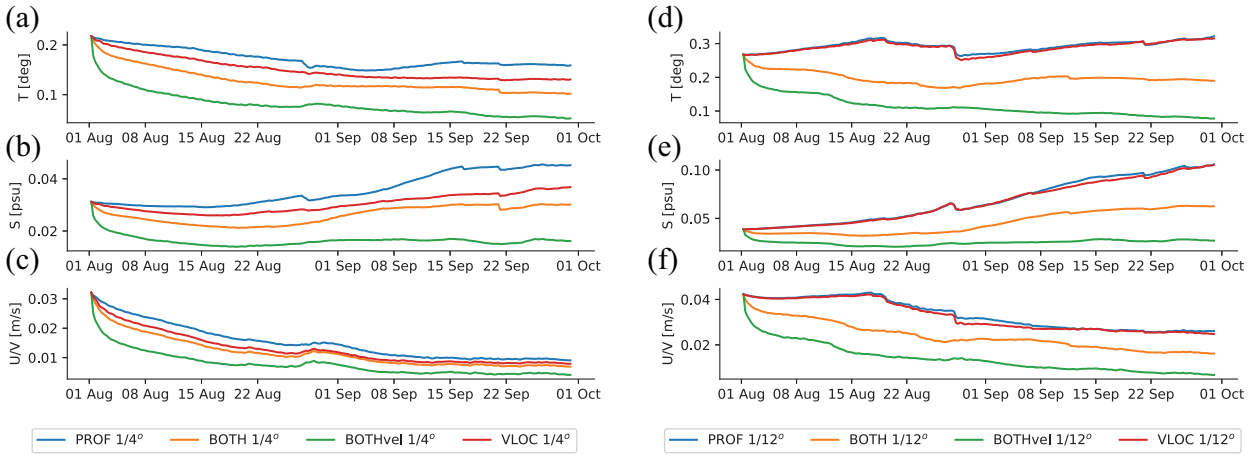

FIG. 13. Time variation of forecast ensemble spreads for DA experiments PROF (blue), BOTH (orange), BOTHvel (green), and VLOC (red): (a) temperature in the 1/4° system, (b) salinity in the 1/4° system, (c) velocity in the 1/4° system, (d) temperature in the 1/12° system, (e) salinity in the 1/12° system, and (f) velocity in the 1/12° system.

avoids the underestimation issue of forecast ensemble spread.

d. *Lagrangian predictability*

In this section we consider the Lagrangian predictability in DA experiments using models with different horizontal resolutions. Two metrics are used to quantify the Lagrangian predictability, which compare the GLAD trajectories with simulated forecast trajectories within the analysis flow fields (Muscarella et al. 2015). The *separation distance* is the geophysical distance (in kilometers) between the positions of the observed and simulated drifters at a specified time:

$$\Delta s = \frac{1}{L_D}\sum_{m=1}^{L_D} d\left[(\lambda_m^o,\ \varphi_m^o),\ \left(\overline{\lambda}_m^f,\ \overline{\varphi}_m^f\right)\right], \tag{11}$$

where $(\lambda_m^o,\ \varphi_m^o)$ is the observed GPS location of the mth GLAD drifter, and $\left(\overline{\lambda}_m^f,\ \overline{\varphi}_m^f\right)$ is the ensemble mean forecasted location of the same drifter.

For both the eddy-permitting and eddy-resolving model configurations (Fig. 14), the experiments assimilating additional surface drifter positions (BOTH and VLOC) produce smaller separation distances than the experiment assimilating only temperature and salinity profiles (PROF). The application of vertical localization reduces the separation distances compared to the experiments assimilating only profiles (PROF) using both the 1/4° and 1/12° model configurations by 24% and 14%, respectively. Meanwhile, VLOC demonstrates marginally less forecast accuracy in Lagrangian distances than the assimilation of both profiles and drifter positions without vertical localization (BOTH), which coincides with the results of Fig. 12. In addition, for the experiment BOTH, increasing the horizontal resolution alleviates a sudden increase of

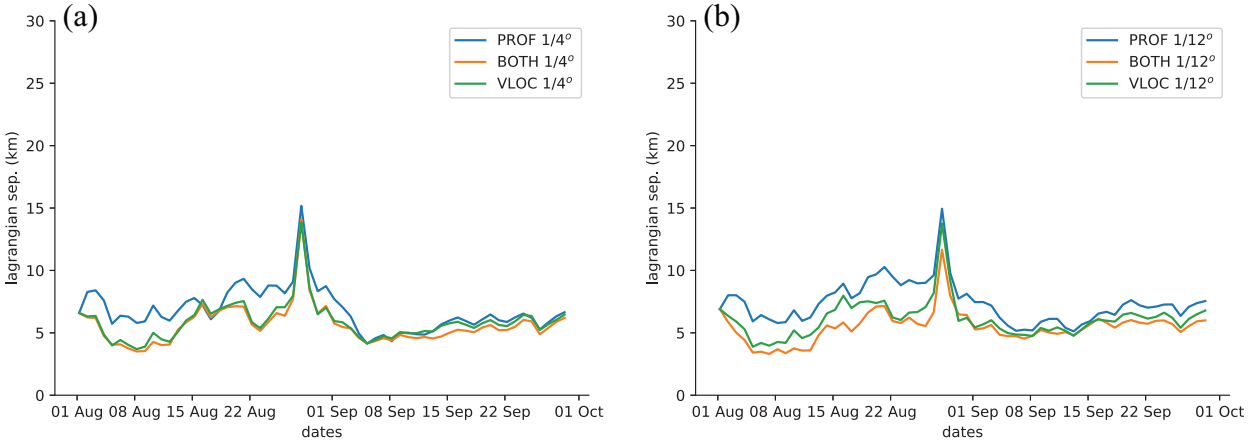

FIG. 14. Average separation distance (km) between the observed drifter position and the simulated drifter positions generated from experiments PROF (blue), BOTH (orange), and VLOC (green) runs of horizontal resolutions in (a) 1/4° and (b) 1/12°.

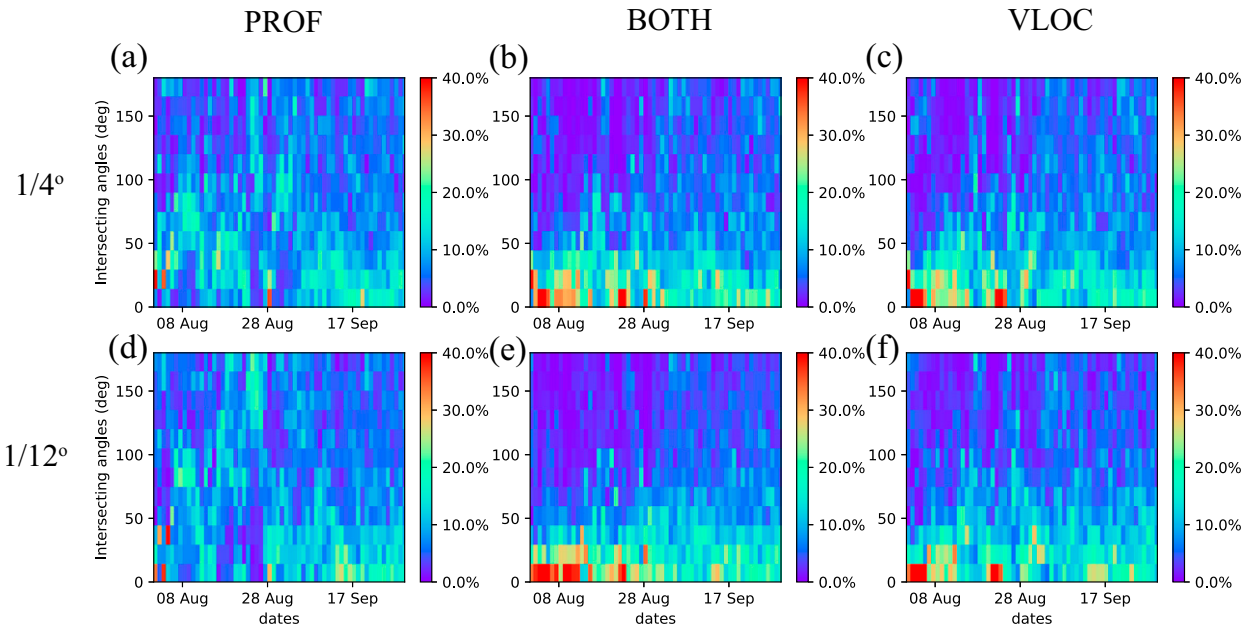

FIG. 15. Comparisons of the occurrence frequency for angle differences in percentage for experiments: (a),(d) PROF; (b),(e) BOTH; and (c),(f) VLOC of horizontal resolution (top) 1/4° and (bottom) 1/12° (the occurrence frequency are averaged daily). Within every panel, each column of pixels shows a distribution of the angle differences between the observed and the simulated drifter moving direction. The cases assimilating the additional surface drifter positions (BOTH and VLOC) show more instances of simulated drifters aligning with observed drifter trajectories.

separation distance on 28 Aug. 2012 while Hurricane Isaac (2012) was passing through the GoM.

The *angular difference* is used to determined possible direction biases along the drifter path:

$$\Delta\theta_m = \cos^{-1}\left(\frac{\mathbf{v}_m^f \cdot \mathbf{v}_m^o}{\|\mathbf{v}_m^f\|\|\mathbf{v}_m^o\|}\right), \quad m = 1, 2, \ldots, L_D, \tag{12}$$

where $\mathbf{v}_m^f$ and $\mathbf{v}_m^o$ are vectors originating from the same initial location at the observed positions from the previous time step, and terminating at the corresponding forecasted and observed positions, respectively.

As the angular difference ranges from 0° to 180°, we evenly divide the range into 12 bins and consider the time variation of the occurrence frequency for each bin during the whole DA process. Figure 15 shows the occurrence frequency (in percentage) of angular differences throughout all of the experiments that fall within a given time range. On average more than 50% of angular differences fall within the bins for small angular differences (less than or equal to 45°) in BOTH and VLOC for different horizontal resolutions (i.e., 53% in 1/4° BOTH, 57% in 1/12° BOTH, 50% in 1/4° VLOC and 51% in 1/12° VLOC), compared with 36% and 35% in the PROF experiments. For experiments assimilating only profiles (PROF), the angular differences are widely distributed in different angle bins, in which obtuse angles (greater than 90°) occupy a relatively larger percentage than BOTH and VLOC during the experiment period. This implies that the BOTH and VLOC experiments at different resolutions provide more accuracy in estimating the true flow direction at the ocean surface.

6. Discussion and outlook

An application of the augmented-state Lagrangian data assimilation (LaDA) using LETKF (LETKF-LaDA; Sun and Penny 2019) within a realistic ocean DA framework has been investigated for the Gulf of Mexico. We assimilated historical data, including in situ temperature and salinity profiles from the WOD18 as well as surface drifter positions and derived velocities from the GLAD field experiment. We investigated the impacts of LaDA on two types forecast models: 1) an eddy-permitting ocean model with 1/4° horizontal resolution, and 2) an eddy-resolving ocean model with 1/12° horizontal resolution. Compared with assimilating only conventional in situ temperature and salinity profiles, the additional LaDA of surface drifter position measurements improved estimates of the synoptic ocean surface velocity at different horizontal resolutions. The advantage of LaDA was particularly notable while Hurricane Isaac (2012) impacted the GoM (26–30 August). In this case, assimilating surface drifter positions using LaDA led to greater accuracy than assimilating derived Eulerian velocity measurements in the estimation of temperature and salinity fields ranging from the surface to the deep layers. It is also shown that LaDA has greater advantages in characterizing the velocity fields of the fast advective ocean currents than the Eulerian approach. This improved accuracy was amplified as the horizontal model resolution was increased from 1/4° to 1/12°. As there is a growing interest in better resolving ocean surface currents to improve the forecast of tropical cyclones (e.g., Li and Toumi 2018; Zhang and Emanuel 2018; Chen and Zhang 2019; Phillipson et al. 2021), this suggests a potential

use for the augmented-state LaDA in applications of the extreme weather conditions like tropical cyclones.

As for the estimation of the synoptic temperature and salinity fields, the additional assimilation of surface drifter positions can degrade RMSEs below the mixed layer depth, compared to assimilating only in situ temperature and salinity profiles. This degradation was eliminated by applying a vertical localization to the assimilation of surface drifter positions, thus recovering similar accuracy below the mixed layer depth. Using the 1/12° model resolution with a combination of vertically localized LaDA of drifter positions and conventional assimilation of temperature and salinity profiles resulted in the most accurate estimates of temperature and salinity below mixed layer depth. In addition, experiments using LaDA resulted in substantially improved predictability of drifter trajectories compared to experiments assimilating only in situ profiles.

As a first study on the realistic application of the LETKF-LaDA, we focused on the potential benefits of adding the assimilation of surface drifter positions measured with GPS sensors to a conventional assimilation of in situ temperature and salinity profile observations. Because of the limited experiment duration of GLAD, we were unable to examine the LETKF-LaDA for an extended period. Future efforts will investigate the performance of LETKF-LaDA for a long duration experiment scenario and will include the assimilation of additional observational datasets such as satellite SST, altimeter data, and Global Drifter Program surface drifters equipped with temperature and salinity sensors. Due to the limitation that GLAD drifter observations only cover a partial region of the GoM, we only discuss the improvement at the center of the GoM, which cannot cover the whole Loop Current system. As the deploying range of surface drifters is enlarged in the future, the impacts of LaDA on the estimation of surface currents in Loop Current and transporting water mass from straits of Florida and Yucatan Current can be further investigated.

Acknowledgments. LS and SGP acknowledge support from the NOAA Climate Program Office (CPO) (NA16OAR4310140), the NOAA Next Generation Global Prediction System (NGGPS) program (NA18NWS4680048), and the Indian Institute of Tropical Meteorology (IITM) Monsoon Mission II (MM-II) (IITMMMIIUNIVMARYLANDUSA2018INT2). SGP further acknowledges support from the Office of Naval Research Grants N00014-19-1-2522 and N00014-20-1-2580, and NOAA Grants NA18NWS4680048, NA19NES4320002, and NA20OAR4600277. Resources supporting this work were provided by the Aditya High Performance Computing at the IIM. The SODA dataset of version 3.4.1 used in this research is publicly available (http://www.atmos.umd.edu/~ocean/index_files/soda3.4.1_mn_download.htm). The GLAD dataset is publicly available (https://data.gulfresearchinitiative.org/data/R1.x134.073:0004).

Data availability statement. Datasets for this research are archived on the Indian Institute of Tropical Meteorology High Performance System Aaditya (http://aadityahpc.tropmet.res.in/Aaditya/index.html) and are available upon request to the authors.

REFERENCES

Adcroft, A., and Coauthors, 2019: The GFDL global ocean and sea ice model OM4.0: Model description and simulation features. *J. Adv. Model. Earth Syst.*, **11**, 3167–3211, https://doi.org/10.1029/2019MS001726.

Apte, A., and C. K. R. T. Jones, 2013: The impact of nonlinearity in Lagrangian data assimilation. *Nonlinear Processes Geophys.*, **20**, 329–341, https://doi.org/10.5194/npg-20-329-2013.

——, ——, and A. M. Stuart, 2008: A Bayesian approach to Lagrangian data assimilation. *Tellus*, **60A**, 336–347, https://doi.org/10.1111/j.1600-0870.2007.00295.x.

Bailey, K., and Coauthors, 2019: Coastal mooring observing networks and their data products: Recommendations for the next decade. *Front. Mar. Sci.*, **6**, 180, https://doi.org/10.3389/fmars.2019.00180.

Berta, M., A. Griffa, and M. G. Magaldi, 2015: Improved surface velocity and trajectory estimates in the Gulf of Mexico from blended satellite altimetry and drifter data. *J. Atmos. Oceanic Technol.*, **32**, 1880–1901, https://doi.org/10.1175/JTECH-D-14-00226.1.

Bishop, C. H., B. J. Etherton, and S. J. Majumdar, 2001: Adaptive sampling with the ensemble transform Kalman filter. Part I: Theoretical aspects. *Mon. Wea. Rev.*, **129**, 420–436, https://doi.org/10.1175/1520-0493(2001)129<0420:ASWTET>2.0.CO;2.

Bojinski, S., M. Verstraete, T. C. Peterson, C. Richter, A. Simmons, and M. Zemp, 2014: The concept of essential climate variables in support of climate research, applications, and policy. *Bull. Amer. Meteor. Soc.*, **95**, 1431–1443, https://doi.org/10.1175/BAMS-D13-00047.1.

Capodici, F., and Coauthors, 2019: Validation of HF radar sea surface currents in the Malta-Sicily channel. *Remote Sens. Environ.*, **225**, 65–76, https://doi.org/10.1016/j.rse.2019.02.026.

Carrier, M. J., H. Ngodock, S. Smith, G. Jacobs, P. Muscarella, T. Ozgokmen, B. Haus, and B. Lipphardt, 2014: Impact of assimilating ocean velocity observations inferred from Lagrangian drifter data using the NCOM-4DVAR. *Mon. Wea. Rev.*, **142**, 1509–1524, https://doi.org/10.1175/MWR-D-13-00236.1.

——, H. E. Ngodock, P. Muscarella, and S. Smith, 2016: Impact of assimilating surface velocity observations on the model sea surface height using the NCOM-4DVAR. *Mon. Wea. Rev.*, **144**, 1051–1068, https://doi.org/10.1175/MWR-D-14-00285.1.

Carton, J. A., G. A. Chepurin, and L. Chen, 2018a: SODA3: A new ocean climate reanalysis. *J. Climate*, **31**, 6967–6983, https://doi.org/10.1175/JCLI-D-18-0149.1.

——, ——, ——, and S. A. Grodsky, 2018b: Improved global net surface heat flux. *J. Geophys. Res. Oceans*, **123**, 3144–3163, https://doi.org/10.1002/2017JC013137.

Chelton, D., R. A. deSzoeke, M. G. Schlax, K. El Nagger, and N. Siwertz, 1998: Geophysical variability of the first baroclinic Rossby radius of deformation. *J. Phys. Oceanogr.*, **28**, 433–460, https://doi.org/10.1175/1520-0485(1998)028<0433:GVOTFB>2.0.CO;2.

Chen, X., and F. Zhang, 2019: Development of a convection-permitting air-sea-coupled ensemble data assimilation system for tropical cyclone prediction. *J. Adv. Model. Earth Syst.*, **11**, 3474–3496, https://doi.org/10.1029/2019MS001795.

Coelho, E. F., and Coauthors, 2015: Ocean current estimation using a multi-model ensemble Kalman filter during the Grand

LAgrangian Deployment experiment (GLAD). *Ocean Modell.*, **87**, 86–106, https://doi.org/10.1016/j.ocemod.2014.11.001.

De Cruz, L., J. Demaeyer, S. Vannitsem, S. Schubert, and V. Lucarini, 2018: Exploring the Lyapunov instability properties of high-dimensional atmospheric and climate models. *Nonlinear Processes Geophys.*, **25**, 387–412, https://doi.org/10.5194/npg-25-387-2018.

Delandmeter, P., and E. van Sebille, 2019: The Parcels v2.0 Lagrangian framework: New field interpolation schemes. *Geosci. Model Dev.*, **12**, 3571–3584, https://doi.org/10.5194/gmd-12-3571-2019.

Evensen, G., 2004: Sampling strategies and square root analysis schemes for the EnKF with correction. *Ocean Dyn.*, **54**, 539–560, https://doi.org/10.1007/s10236-004-0099-2.

Flather, R. A., and N. S. Heaps, 1975: Tidal computations for Morecambe Bay. *Geophys. J. Int.*, **42**, 489–517, https://doi.org/10.1111/j.1365-246X.1975.tb05874.x.

Garcia, H. E., T. P. Boyer, R. A. Locarnini, O. K. Baranova, and M. M. Zweng, 2018: World Ocean Database 2018: User's manual (prerelease). NOAA, Silver Spring, MD, 109 pp., https://rda.ucar.edu/datasets/ds285.0/docs/WOD18-UsersManual_final.pdf.

Greybush, S. J., E. Kalnay, T. Miyoshi, K. Ide, and B. Hunt, 2011: Balance and ensemble Kalman filter localization techniques. *Mon. Wea. Rev.*, **139**, 511–522, https://doi.org/10.1175/2010MWR3328.1.

Griffes, S. M., and Coauthors, 2015: A historical introduction to MOM. NOAA/Geophysical Fluid Dynamics Laboratory, 24 pp., https://www.gfdl.noaa.gov/wp-content/uploads/2019/04/mom_history_2017.09.19.pdf.

Hamill, T. M., J. S. Whitaker, and C. Snyder, 2001: Distance-dependent filtering of background error covariance estimates in an ensemble Kalman filter. *Mon. Wea. Rev.*, **129**, 2776–2790, https://doi.org/10.1175/1520-0493(2001)129,2776:DDFOBE.2.0.CO;2

Haza, A. C., T. M. Ozgokmen, A. Griffa, A. C. Poje, and M.-P. Lelong, 2014: How does drifter position uncertainty affect ocean dispersion estimates? *J. Atmos. Oceanic Technol.*, **31**, 2809–2828, https://doi.org/10.1175/JTECH-D-14-00107.1.

Hernandez, F., P.-Y. Le Traon, and N. H. Barth, 1995: Optimizing a drifter cast strategy with a genetic algorithm. *J. Atmos. Oceanic Technol.*, **12**, 330–345, https://doi.org/10.1175/1520-0426(1995)012<0330:OADCSW>2.0.CO;2.

Hunt, B. R., E. J. Kostelich, and I. Szunyogh, 2007: Efficient data assimilation for spatiotemporal chaos: A local ensemble transform Kalman filter. *Physica D*, **230**, 112–126, https://doi.org/10.1016/j.physd.2006.11.008.

Ide, K., L. Kuznetsov, and C. K. R. T. Jones, 2002: Lagrangian data assimilation for point-vortex system. *J. Turbul.*, **3**, 053, https://doi.org/10.1088/1468-5248/3/1/053.

Isern-Fontanet, J., J. Ballabrera-Poy, and A. Turiel, 2017: Remote sensing of ocean surface currents: A review of what is being observed and what is being assimilated. *Nonlinear Processes Geophys.*, **24**, 613–643, https://doi.org/10.5194/npg-24-613-2017.

Ishikawa, Y., T. Awaji, K. Akitomo, and B. Qiu, 1996: Successive correction of the mean sea surface height by the simultaneous assimilation of drifting buoy and altimetric data. *J. Phys. Oceanogr.*, **26**, 2381–2397, https://doi.org/10.1175/1520-0485(1996)026<2381:SCOTMS>2.0.CO;2.

Jacobs, G., and Coauthors, 2014: Data assimilation considerations for improved ocean predictability during the Gulf of Mexico Grand Lagrangian Deployment (GLAD). *Ocean Modell.*, **83**, 98–117, https://doi.org/10.1016/j.ocemod.2014.09.003.

Jazwinski, A. H., 1970: *Stochastic Processes and Filtering Theory*. Academic Press, 376 pp.

Kuznetsov, L., K. Ide, and C. K. R. T. Jones, 2003: A method for assimilation of Lagrangian data. *Mon. Wea. Rev.*, **131**, 2247–2260, https://doi.org/10.1175/1520-0493(2003)131<2247:AMFAOL>2.0.CO;2.

Li, Y., and R. Toumi, 2018: Improved tropical cyclone intensity forecasts by assimilating coastal surface currents in an idealized study. *Geophys. Res. Lett.*, **45**, 10 019–10 026, https://doi.org/10.1029/2018GL079677.

Mohamad, M. A., and A. J. Majda, 2020: Recovering the Eulerian energy spectrum from noisy Lagrangian tracers. *Physica D*, **403**, 132374, https://doi.org/10.1016/j.physd.2020.132374.

Molcard, A., L. I. Piterbarg, A. Griffa, T. M. Özgökmen, and A. J. Mariano, 2003: Assimilation of drifter positions for the reconstruction of the Eulerian circulation field. *J. Geophys. Res.*, **108**, 3056, https://doi.org/10.1029/2001JC001240.

——, A. Griffa, and T. M. Özgökmen, 2005: Lagrangian data assimilation in multi-layer primitive equation ocean models. *J. Atmos. Oceanic Technol.*, **22**, 70–83, https://doi.org/10.1175/JTECH-1686.1.

Muscarella, P., M. J. Carrier, H. Ngodock, S. Smith, B. L. Lipphardt, A. D. Kirwan, and H. S. Huntley, 2015: Do assimilated drifter velocities improve Lagrangian predictability in an operational ocean model? *Mon. Wea. Rev.*, **143**, 1822–1832, https://doi.org/10.1175/MWR-D-14-00164.1.

Nilsson, J. A. U., S. Dobricic, N. Pinardi, P. M. Poulain, and D. Pettenuzzo, 2012: Variational assimilation of Lagrangian trajectories in the Mediterranean Ocean forecasting system. *Ocean Sci.*, **8**, 249–259, https://doi.org/10.5194/os-8-249-2012.

NOAA/GFDL, 2021: Welcome to MOM6;s documentation. NOAA/GFDL, accessed 12 May 2021, https://mom6.readthedocs.io/en/dev-gfdl/.

Nodet, M., 2006: Variational assimilation of Lagrangian data in oceanography. *Inverse Probl.*, **22**, 245–263, https://doi.org/10.1088/0266-5611/22/1/014.

Ott, E., and Coauthors, 2004: A local ensemble Kalman filter for atmospheric data assimilation. *Tellus*, **56A**, 415–428, https://onlinelibrary.wiley.com/doi/abs/10.1111/j.1600-0870.2004.00076.x.

Orlanski, I., 1976: A simple boundary condition for unbounded hyperbolic flows. *J. Comput. Phys.*, **21**, 251–269, https://doi.org/10.1016/0021-9991(76)90023-1.

Özgökmen, T., 2013: GLAD experiment CODE-style drifter trajectories (low-pass filtered, 15 minute interval records), northern Gulf of Mexico near DeSoto Canyon, July–October 2012. Gulf of Mexico Research Initiative Information and Data Cooperative (GRIIDC), Harte Research Institute, Texas A&M University–Corpus Christi, accessed 7 April 2022, https://doi.org/10.7266/N7VD6WC8.

——, A. Molcard, T. M. Chin, L. I. Piterbarg, and A. Griffa, 2003: Assimilation of drifter observations in primitive equation models of midlatitude ocean circulation. *J. Geophys. Res.*, **108**, 3238, https://doi.org/10.1029/2002JC001719.

Palatella, L., 2013: Lyapunov vectors and assimilation in the unstable subspace: Theory and applications. *J. Phys. A Math. Theor.*, **46**, 254020, https://doi.org/10.1088/1751-8113/46/25/254020.

Pearson, J., B. Fox-Kemper, R. Barkan, J. C. Mcwilliams, J. Choi, and A. Bracco, 2019: Impacts of convergence on structure functions from surface drifters in the Gulf of Mexico. *J. Phys. Oceanogr.*, **49**, 675–690, https://doi.org/10.1175/JPO-D-18-0029.1.

Penny, S. G., and T. Miyoshi, 2016: A local particle filter for high-dimensional geophysical systems. *Nonlinear Processes Geophys.*, **23**, 391–405, https://doi.org/10.5194/npg-23-391-2016.

——, D. W. Behringer, J. A. Carton, and E. Kalnay, 2015: A hybrid global ocean data assimilation system at NCEP. *Mon. Wea. Rev.*, **143**, 4660–4677, https://doi.org/10.1175/MWR-D-14-00376.1.

——, E. Bach, K. Bhargava, C.-C. Chang, C. Da, L. Sun, and T. Yoshida, 2019: Strongly coupled data assimilation in multiscale media: Experiments using a quasi-geostrophic coupled model. *J. Adv. Model. Earth Syst.*, **11**, 1803–1829, https://doi.org/10.1029/2019MS001652.

Phillipson, L., and R. Toumi, 2017: Impact of data assimilation on ocean current forecasts in the Angola basin. *Ocean Modell.*, **114**, 45–58, https://doi.org/10.1016/j.ocemod.2017.04.006.

——, Y. Li, and R. Toumi, 2021: Strongly coupled assimilation of a hypothetical ocean current observing network within a regional ocean-atmosphere coupled model: An OSSE case study of typhoon Hato. *Mon. Wea. Rev.*, **149**, 1317–1336, https://doi.org/10.1175/MWR-D-20-0108.1.

Poje, A. C., and Coauthors, 2014: Submesoscale dispersion in the vicinity of the *Deepwater Horizon* Spill. *Proc. Natl. Acad. Sci. USA*, **111**, 12 693–12 698, https://doi.org/10.1073/pnas.1402452111.

Salman, H., 2008a: A hybrid grid/particle filter for Lagrangian dataassimilation. I: Formulating the passive scalar approximation. *Quart. J. Roy. Meteor. Soc.*, **134**, 1539–1550, https://doi.org/10.1002/qj.270.

——, 2008b: A hybrid grid/particle filter for Lagrangian data assimilation. II: Application to a model vortex flow. *Quart. J. Roy. Meteor. Soc.*, **134B**, 1551–1565, https://doi.org/10.1002/qj.279.

——, L. Kuznetsov, C. K. R. T. Jones, and K. Ide, 2006: A method for assimilating Lagrangian data into a shallow-water-equation ocean model. *Mon. Wea. Rev.*, **134**, 1081–1101, https://doi.org/10.1175/MWR3104.1.

——, C. K. R. T. Jones, and K. Ide, 2008: Using flow geometry for drifter deployment in Lagrangian data assimilation. *Tellus*, **60A**, 321–335, https://doi.org/10.1111/j.1600-0870.2007.00292.x.

Santoki, M., K. N. Joshipura, S. Ratheesh, R. Sharma, and S. Basu, 2012: Assimilation of drifter data in a circulation model of the Indian Ocean. *IEEE Geosci. Remote Sens. Lett.*, **9**, 100–103, https://doi.org/10.1109/LGRS.2011.2161455.

——, S. George, and R. Sharma, 2013: Assimilation of satellite-derived ocean surface current in an Indian Ocean circulation model. *Remote Sens. Lett.*, **4**, 475–484, https://doi.org/10.1080/2150704X.2012.750036.

Scharroo, R., E. W. Leuliette, J. L. Lillibridge, D. Byrne, M. C. Naeije, and G. T. Mitchum, 2013: RADS: Consistent multi-mission products. *Proc. Symp. on 20 Years of Progress in Radar Altimetry*, Venice, Italy, European Space Agency Special Publ. ESA SP-710, 4 pp.

Slivinski, L. C., E. Spiller, A. Apte, and B. Sandstede, 2015: A hybrid particle–ensemble Kalman filter for Lagrangian data assimilation. *Mon. Wea. Rev.*, **143**, 195–211, https://doi.org/10.1175/MWR-D-14-00051.1.

——, and Coauthors, 2019: Towards a more reliable historical reanalysis: Improvements for version 3 of the Twentieth Century Reanalysis System. *Quart. J. Roy. Meteor. Soc.*, **145**, 2876–2908, https://doi.org/10.1002/qj.3598.

Snyder, C., T. Bengtsson, P. Bickel, and J. Anderson, 2008: Obstacles to high-dimensional particle filtering. *Mon. Wea. Rev.*, **136**, 4629–4640, https://doi.org/10.1175/2008MWR2529.1

Spiller, E., A. Budhiraja, K. Ide, and C. Jones, 2008: Modified particle filter methods for assimilating Lagrangian data into a point-vortex model. *Physica D*, **237**, 1498–1506, https://doi.org/10.1016/j.physd.2008.03.023.

Sun, L., and S. G. Penny, 2019: Lagrangian data assimilation of surface drifters in a double-gyre ocean model using the local ensemble transform Kalman filter. *Mon. Wea. Rev.*, **147**, 4533–4551, https://doi.org/10.1175/MWR-D-18-0406.1.

Taillandier, V., A. Griffa, and A. Molcard, 2006: A variational approach for the reconstruction of regional scale Eulerian velocity fields from Lagrangian data. *Ocean Modell.*, **13**, 1–24, https://doi.org/10.1016/j.ocemod.2005.09.002.

Toner, M., A. D. Kirwan, L. H. Kantha, and J. K. Choi, 2001a: Can general circulation models be assessed and their output enhanced with drifter data. *J. Geophys. Res. Oceans*, **106**, 563–19, https://doi.org/10.1029/2000JC000587.

——, A. C. Poje, A. D. Kirwan, C. K. R. T. Jones, B. L. Lipphardt, and C. E. Grosch, 2001b: Reconstructing basin-scale Eulerian velocity fields from simulated drifter data. *J. Phys. Oceanogr.*, **31**, 1361–1376, https://doi.org/10.1175/1520-0485(2001)031<1361:RBSEVF>2.0.CO;2.

Trevisan, A., and L. Palatella, 2011: On the Kalman filter error covariance collapse into the unstable subspace. *Nonlinear Processes Geophys.*, **18**, 243–250, https://doi.org/10.5194/npg-18-243-2011.

——, M. D'Isidoro, and O. Talagrand, 2010: Four-dimensional variational assimilation in the unstable subspace and the optimal subspace dimension. *Quart. J. Roy. Meteor. Soc.*, **136**, 487–496, https://doi.org/10.1002/qj.571.

Vernieres, G., C. K. R. T. Jones, and K. Ide, 2011: Capturing eddy shedding in the Gulf of Mexico from Lagrangian observations. *Physica D*, **240**, 166–179, https://doi.org/10.1016/j.physd.2010.06.008.

Wallcraft, A. J., E. J. Metzger, and S. N. Carroll, 2009: Software design description for the HYbrid Coordinate Ocean Model (HYCOM) version 2.2. Memo. Rep. ADA494779, Naval Research Lab Stennis Space Center, MS, 157 pp., https://apps.dtic.mil/sti/citations/ADA494779.

WMO, 2015: Status of the global observing system for climate. WMO Rep. GCOS195, World Meteorological Society, Geneva, Switzerland, 373 pp.

Zhang, F., and K. Emanuel, 2018: Promises in air-sea fully coupled data assimilation for future hurricane prediction. *Geophys. Res. Lett.*, **45**, 173–13, https://doi.org/10.1029/2018GL080970.